RENDEZVOUS INVOLVING A NON-COOPERATIVE, TUMBLING TARGET - ESTIMATION OF MOMENTS OF INERTIA AND CENTER OF MASS OF AN UNKNOWN TARGET

Heike Benninghoff[(1)] **and Toralf Boge**[(2)]
[(1)]*German Aerospace Center (DLR), 82234 Wessling, +49 8153 28-1465, Heike.Benninghoff@dlr.de*
[(2)]*German Aerospace Center (DLR), 82234 Wessling, +49 8153 28-2485, Toralf.Boge@dlr.de*

Abstract: *Safe approach and docking to a non-cooperative, tumbling target satellite is one of the main critical issues in on-orbit servicing missions. Knowledge of the inertia properties of the target spacecraft is a prerequisite for many rendezvous and docking aspects. In this paper we propose a method to estimate the center of mass and moments of inertia using optical sensor data. For that, kinematic equations of motion and the conservation of the angular momentum are employed to estimate the unknown quantities with least squares methods. Observability and limitations are discussed and results gained from computer simulations involving different test cases are presented.*

Keywords: *On-orbit servicing, inertia parameter estimation, non-cooperative target, GN&C, autonomous navigation.*

1. Introduction

In on-orbit servicing missions, a service spacecraft approaches an non-cooperative, passive target spacecraft in its orbit to perform service tasks. These can comprise lifetime extensions tasks like takeover of orbit and attitude control, refueling, reparations or space debris removal actions like safe deorbiting at the target spacecraft's end of life [1, 2, 3, 4]. The rendezvous and capture of the client spacecraft are critical phases in an on-orbit servicing mission and induce a large research area on guidance, navigation and control [5, 6, 7, 8].

A typical non-cooperative target satellite is neither equipped with reflectors or markers which can be used for relative navigation, nor has specially intended grasping/docking equipment for robotic capture [5]. Furthermore, there is no communication between servicing and target satellite or between ground station and target. Therefore, the status of the target has to be assumed as fully unknown. This means that there is no information about the target's pose (position and orientation) and none about its inertia properties, which is necessary to propagate its state.

For a safe approach to and capture of the target, knowledge of the inertia properties is important. For example, the motion of a possible grasping point on the target's side has to be propagated for planning a safe capture process. Further, having the target grasped, its motion has to be damped which is not possible without any knowledge of its inertia properties. Consequently, we have to determine the location of the center of mass of the body and its moments of inertia during a previous inspection phase carried out at a safe distance. Fig. 1 shows a tumbling client satellite observed during such an inspection phase with three different poses.

As the target is uncooperative, we cannot control its attitude during the inspection phase. This is

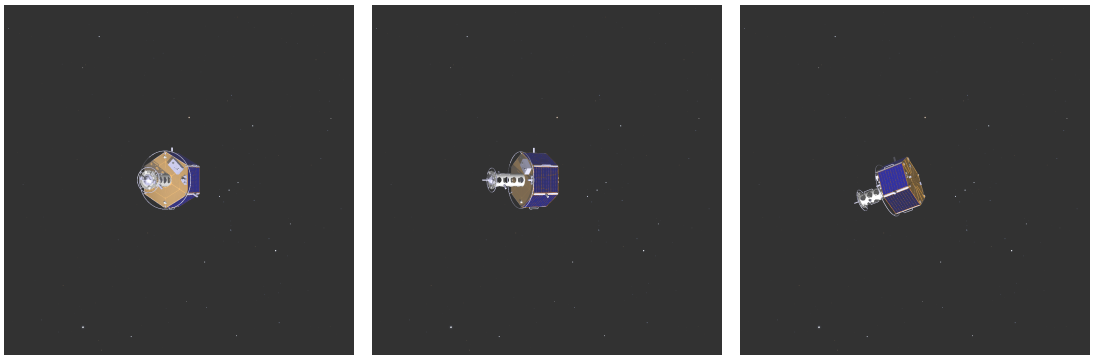

Figure 1. Inspection phase during an on-orbit servicing mission: Observation of a tumbling target from a safe distance for determination of its inertia parameters.

why existing approaches [9, 10, 11, 12] for in-flight estimation of the inertia parameters cannot be applied. The main idea of those methods is to apply torque on the satellite using reaction wheels or a robotic arm followed by an investigation of the induced rotational motion.

In the on-orbit servicing scenario, we need to make use of information which can be gained using the available equipment on the service satellite only [13, 14]. Therefore, optical sensors such as CCD or CMOS cameras or time-of-flight sensors like LIDARs (LIght Detection And Ranging) mounted on the service spacecraft can be used. From a safe distance, the free-tumbling target satellite is observed and the inertia properties of the unknown target can be estimated using the processed sensor data. Processing the data of optical sensors, the position of the center of some geometrical body frame of the target and its orientation can be measured. The center of mass may not match with the geometrical center. One task is to determine the shift between geometrical center and center of mass.

In this work, we assume that the target is freely rotating without any external torque acting on it. As in [15], the center of mass and the moments of inertia can be determined using kinematic equations and the conservation of angular momentum. As the angular momentum in an inertial reference frame is constant but unknown, it is estimated together with the inertia tensor. By using a high number of measurements of optical sensors gained during an inspection, least square problems are solved to estimate the optimal center of mass and inertia parameters which best fit to the measurements.

In summary, the objective of this paper is to estimate the center of mass and the moments of inertia of a non-cooperative, tumbling target using measurements of optical sensors mounted on the service satellite.

Additionally to the approach presented in [15], we take constraints on the moments of inertia into account to enforce positive diagonal entries in the inertia matrix. This induces a minimization problem with inequality constraints which can be solved using the active set method for convex quadratic programming [16]. In addition, singular value decomposition of matrices is applied to overcome problems arising from numerical issues and errors. We investigate the performance of the method, discuss limitations in the observability, and analyze the influence of e.g. the number of measurements on the performance.

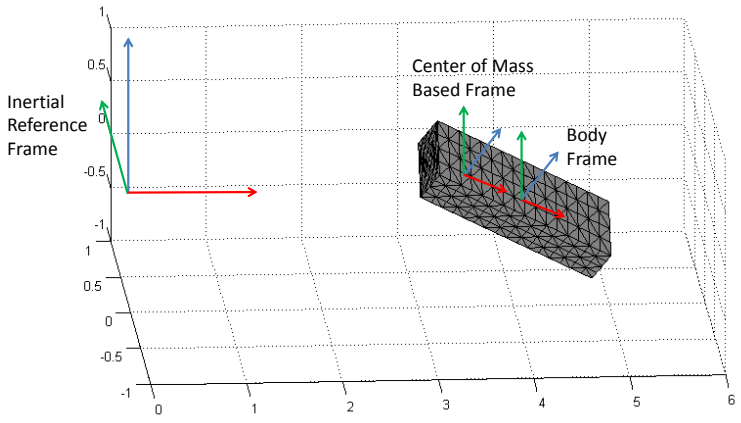

Figure 2. Overview on the coordinate frames (x-axis: red, y-axis: green, z-axis: blue)

2. Methods and Theoretical Aspects

In this section, a method to estimate the center of mass and the moments of inertia of a tumbling satellite is presented followed by an analysis of the observability of the quantities.

2.1. Preliminaries

We introduce the following coordinate systems:

Inertial Reference Frame (IRF): A world coordinate frame in which the Newton's laws of motion are valid. The motion of the target, considered as a rigid body, is observed and measured with respect to the inertial reference system.

Body Fixed Coordinate Frame/ Body Frame (BF): A coordinate system fixed to the body. The origin is defined fixed with respect to the body. For example, the origin can be set to the geometrical center if the geometry of the rigid body is of simple nature, e.g. if it is cylinder- or cuboid-like.

Center of Mass Based Coordinate Frame (CMF): A coordinate system with the center of mass being the origin. Its coordinate axes are parallel to those of the Body Fixed Coordinate System. For example, for a homogeneous mass distribution, BF and CMF are identical.

For the ease of notation, the origin of the Body Frame is denoted as *geometrical center* of the body in this paper. Fig. 2 visualizes the coordinate frames: The inertial reference frame is fixed. The body and center of mass based frames are moving and rotating with the body.

We assume that N measurements of the following quantities are provided by an optical sensor and its processing unit:

- The position $\vec{p}_i^{IRF} \in \mathbb{R}^3$, $i = 1,\dots,N$, of the geometrical center of the body measured in IRF.
- The velocity $\vec{v}_i^{IRF} \in \mathbb{R}^3$, $i = 1,\dots,N$, of the geometrical center of the body measured in IRF.
- The orientation of the body given by a rotation matrix $R_{i,IRF}^{BF} \in \mathbb{R}^{3\times3}$, $i = 1,\dots,N$, describing

the rotation from IRF to BF.
- The angular velocity $\vec{\omega}_i^{IRF} \in \mathbb{R}^3$, $i = 1, \ldots, N$, of the rotating body in IRF.

The pair $(\vec{p}_i^{IRF}, R_{i,IRF}^{BF})$ measured at time t_i is called *pose*. Processing data from sensors like cameras or LIDARs typically provides a measurement of the pose only. The translational and angular velocities $\vec{v}_i^{IRF}$ and $\vec{\omega}_i^{IRF}$ have to be determined by numerical differentiation from the position and attitude.

Camera and LIDAR based pose estimation is a large research area [17, 18, 19, 20, 21, 14, 22]. Pose estimation is thus beyond the scope of this paper; we assume that the above listed quantities are given as measurements, and we will focus on the estimation of the inertia parameters.

2.2. Center of Mass Estimation

In this subsection, a method is proposed to compute the center of mass of a rigid body with respect to its body frame. I.e. the translation from Body Fixed Frame to Center of Mass Based Frame is determined. We use the method of Sheinfeld and Rock [15] with slight differences for center of mass determination and consider the following kinematic equation for each measurement $i \in \{1, \ldots, N\}$:

$$\vec{v}_i^{IRF} = \vec{v}_{CoM}^{IRF} + \vec{\omega}_i^{IRF} \times \vec{r}_i^{IRF}, \tag{1}$$

where, as defined in Section 2.1., $\vec{v}_i^{IRF}$ is the velocity of the geometrical center of the body and $\vec{\omega}_i^{IRF}$ is the angular velocity of the body in IRF. Both quantities are related to the i-th measurement.

Further, $\vec{v}_{CoM}^{IRF}$ is the unknown velocity of the center of mass expressed in IRF and $\vec{r}_i^{IRF}$ is the vector in IRF pointing from the center of mass to the geometrical center. Let $\vec{r}^{BF}$ denote the constant vector in BF, related to $\vec{r}_i^{IRF}$ by

$$\vec{r}_i^{IRF} = (R_{i,IRF}^{BF})^T \vec{r}^{BF}, \tag{2}$$

where $R_{i,IRF}^{BF}$ describes the orientation of the body, i.e. the rotation from IRF to BF. The superscript T denotes the transpose of a matrix. The constant vector $\vec{r}^{BF}$ can be expressed as

$$\vec{r}^{BF} = \vec{p}_0^{BF} - \vec{p}_{CoM}^{BF} = -\vec{p}_{CoM}^{BF}. \tag{3}$$

The vector $\vec{p}_0^{BF} = (0,0,0)^T$ is the position of the geometrical center (the origin of the body frame) and $\vec{p}_{CoM}^{BF} \in \mathbb{R}^3$ is the unknown position of the center of mass where both vectors are expressed in the body frame.

In the original work of Sheinfeld and Rock [15], a so-called *feature point* at location $\vec{p}_0^{BF}$ is tracked by the sensor and $\vec{v}_i^{IRF}$ is the velocity of the feature point. Here, we track the geometrical center of the body. Using camera data, one could use also a feature point on the body surface instead of the center point, since visible features can be tracked well from camera images. Using LIDAR data, however, the raw sensor data is a 3D point cloud from which the position of the body has to be reconstructed. The motion of single features of the body can hardly be observed and tracked. Therefore, the position of the geometrical center is computed from the 3D point cloud and some geometrical information/model of the body. Therefore, the geometrical center, the origin of the body frame, is used for $\vec{p}_0^{BF}$.

Inserting Eq. 2 and Eq. 3 in Eq. 1 we obtain for the i-th measurement:

$$\vec{v}_i^{IRF} = \vec{v}_{CoM}^{IRF} - \vec{\omega}_i^{IRF} \times \left((R_{i,IRF}^{BF})^T \vec{p}_{CoM}^{BF} \right), \tag{4}$$

The unknown quantities are $\vec{v}_{CoM}^{IRF}$ and $\vec{p}_{CoM}^{BF}$. Therefore, we set

$$\vec{x} := \begin{pmatrix} \vec{v}_{CoM}^{IRF} \\ \vec{p}_{CoM}^{BF} \end{pmatrix} \in \mathbb{R}^6. \tag{5}$$

The system of measurements Eq. 4 can be rewritten to the following matrix vector form

$$A\vec{x} = \vec{b}, \tag{6}$$

where $A \in \mathbb{R}^{3N \times 6}$, $\vec{b} \in \mathbb{R}^{3N}$ are defined by

$$A = \left(\begin{array}{c|c} \mathrm{Id} & -W_1^{IRF} (R_{1,IRF}^{BF})^T \\ \vdots & \vdots \\ \mathrm{Id} & -W_N^{IRF} (R_{N,IRF}^{BF})^T \end{array} \right), \quad \vec{b} = \begin{pmatrix} \vec{v}_1^{IRF} \\ \vdots \\ \vec{v}_N^{IRF} \end{pmatrix}, \tag{7}$$

where $\mathrm{Id} \in \mathbb{R}^{3\times 3}$ is the identity matrix and $W_i^{IRF} \in \mathbb{R}^{3\times 3}$ is defined by

$$W_i^{IRF} = \begin{pmatrix} 0 & -\omega_{i3}^{IRF} & \omega_{i2}^{IRF} \\ \omega_{i3}^{IRF} & 0 & -\omega_{i1}^{IRF} \\ -\omega_{i2}^{IRF} & \omega_{i1}^{IRF} & 0 \end{pmatrix} \tag{8}$$

using the notation $\vec{\omega}_i^{IRF} = (\omega_{i1}^{IRF}, \omega_{i2}^{IRF}, \omega_{i3}^{IRF})^T$.

The linear system Eq. 6 is overdetermined as $3N \gg 6$. Further, the matrix A and the right hand side $\vec{b}$ are based on measurements and are therefore affected by measurement noise. A solution $\vec{x} \in \mathbb{R}^6$ has to be found which solves the system Eq. 6 in the least squares sense, i.e. such that the l^2-norm of the error, i.e.

$$\vec{x} \mapsto \|A\vec{x} - \vec{b}\|^2 = (A\vec{x} - \vec{b})^T (A\vec{x} - \vec{b}), \tag{9}$$

is minimized.

Having determined a solution $\vec{x} \in \mathbb{R}^6$, the position of the center of mass $\vec{p}_{CoM}^{BF} \in \mathbb{R}^3$ is given by the components 4-6 of the vector $\vec{x}$, cf. Eq. 5.

2.3. Inertia Estimation

2.3.1. Basic Method

The method to determine the inertia tensor of the body is based on the method proposed in [15]. In the absence of external torques the angular momentum $\vec{h}^{IRF}$ in the inertial frame IRF is constant. The angular momentum in the body frame $\vec{h}_i^{BF}$ at time t_i, $i \in \{1, \ldots, N\}$, is defined as

$$\vec{h}_i^{BF} = I\vec{\omega}_i^{BF}, \tag{10}$$

where $I \in \mathbb{R}^{3\times 3}$ is the inertia tensor of the body which should be determined and $\vec{\omega}_i^{BF}$ is the angular velocity expressed in the body frame corresponding to the i-th measurement. Using the relation $R_{i,IRF}^{BF}\vec{h}^{IRF} = \vec{h}_i^{BF}$, we conclude

$$R_{i,IRF}^{BF}\vec{h}^{IRF} = I\vec{\omega}_i^{BF} \tag{11}$$

The angular momentum in IRF $\vec{h}^{IRF} = (h_1^{IRF}, h_2^{IRF}, h_3^{IRF})^T$ is not known and has to be estimated together with I. Let I_{ij}, $i,j = 1,2,3$, denote the matrix entries of I. As I is symmetric, we define the vector of unknowns as

$$\vec{x} = \left(I_{11}, I_{12}, I_{13}, I_{22}, I_{23}, I_{33}, h_1^{IRF}, h_2^{IRF}, h_3^{IRF}\right)^T \in \mathbb{R}^9. \tag{12}$$

Eq. 10 with Eq. 11 can be rewritten to the following linear system:

$$A\vec{x} = \vec{0}, \tag{13}$$

where $A \in \mathbb{R}^{3N\times 9}$ is given by

$$A = \left(\begin{array}{c|c} \Omega_1^{BF} & -R_{1,IRF}^{BF} \\ \vdots & \vdots \\ \Omega_N^{BF} & -R_{N,IRF}^{BF} \end{array}\right) \tag{14}$$

with

$$\Omega_i^{BF} = \begin{pmatrix} \omega_{i1}^{BF} & \omega_{i2}^{BF} & \omega_{i3}^{BF} & 0 & 0 & 0 \\ 0 & \omega_{i1}^{BF} & 0 & \omega_{i2}^{BF} & \omega_{i3}^{BF} & 0 \\ 0 & 0 & \omega_{i1}^{BF} & 0 & \omega_{i2}^{BF} & \omega_{i3}^{BF} \end{pmatrix}. \tag{15}$$

Eq. 13 should be solved in the least squares sense, i.e. the solution $\vec{x} \in \mathbb{R}^9$ should minimize

$$\vec{x} \mapsto \|A\vec{x}\|^2 = (A\vec{x})^T A\vec{x} = \vec{x}^T A^T A\vec{x}. \tag{16}$$

Minimizing this quadratic functional leads to a linear system

$$B\vec{x} = \vec{0}, \tag{17}$$

with $B = A^T A \in \mathbb{R}^{9\times 9}$. As the right hand side is zero, B must have a rank of 8 such that a non-trivial solution of the linear system exists. The solution is unique up to a multiplicative factor. This can also be seen from the equation $R_{i,IRF}^{BF}\vec{h}^{IRF} = I\vec{\omega}_i^{BF}$. If a pair $(I, \vec{h}^{IRF})$ solves this equation, any multiply of it will be another solution of the equation. Therefore, the angular momentum and the inertia tensor can only be determined up to a multiplicative factor.

2.3.2. Improvements of the basic method

In practice, the matrix $B = A^T A$ will often be of rank 9 because of measurement noise and numerical rounding errors in the computation. Therefore, computing A and using a black box solver for the linear equation Eq. 17 will only deliver the trivial solution $\vec{x} = \vec{0}$. To overcome this problem arising from noise and numerical rounding errors, the singular values of B should be analyzed and the singular value closest to zero should be corrected and set to 0.

Let $\tilde{B}$ be the corrected matrix with rank 8. We can reorder the rows in $\tilde{B}$ such that

$$\tilde{B} = \begin{pmatrix} b_{11} & \vec{b}_1^T \\ \vec{b}_1 & B_r \end{pmatrix} \tag{18}$$

with $b_{11} \in \mathbb{R}$, $\vec{b}_1 \in \mathbb{R}^8$, and $B_r \in \mathbb{R}^{8\times 8}$ which is of rank 8. Writing $\vec{x} = (1, \vec{x}_r^T)^T$ leads to the reduced problem

$$B_r \vec{x}_r = -\vec{b}_1 \tag{19}$$

which has a unique solution. The solution space of $\tilde{B}\vec{x} = \vec{0}$ is

$$S = \{\lambda\, (1, \vec{x}_r^T)^T \in \mathbb{R}^9 : \lambda \in \mathbb{R}\}. \tag{20}$$

So far, no restrictions on the solution space have been made. Solving the unconstrained problem, the final inertia matrix could have negative diagonal entries. Therefore we consider the following minimization problem with inequality constraints:

$$\begin{aligned} &\text{minimize } q(\vec{x}_r) = \frac{1}{2}\vec{x}_r^T B_r \vec{x}_r + \vec{b}_1^T \vec{x}_r, \quad \text{subject to} \\ &(\vec{x}_r)_j \geq 0 \quad \forall j \in J = \{3,5\}. \end{aligned} \tag{21}$$

Recall the definition of $\vec{x}$, the vector of unknowns, see Eq. 12. The first six components of $\vec{x}$ and the first five components of the reduced vector $\vec{x}_r$ are related to components of the inertia matrix. By setting the first component of $\vec{x}$ to 1, the scaling factor λ has to be positive, and the components 3 and 5 of $\vec{x}_r$, which are related to I_{22}/I_{11} and I_{33}/I_{11}, have to be positive as well.

A solution of Eq. 21 can be computed using an appropriate numerical optimization method. In the results presented in Section 3., we used the active set method for convex quadratic programming [16].

2.3.3. Summary of the Algorithm

The procedure for inertia estimation can be summarized as follows:

1. Compute the matrix A as defined in Eq. 14. Set $B = A^T A$.
2. Compute a singular value decomposition $B = USV^T$, where U and V are orthogonal matrices and S is a diagonal matrix.
3. Let $\sigma_1 \geq \sigma_2 \geq \ldots \geq \sigma_9 \geq 0$ denote the diagonal entries of S. Let $\tilde{S}$ denote the modified matrix obtained from S by setting the smallest singular value to zero, i.e. $\sigma_9 = 0$. Set $\tilde{B} = U\tilde{S}V^T$.
4. Compute the solution $\vec{x}_r \in \mathbb{R}^8$ of the constrained quadratic problem Eq. 21 and set $\vec{x} = (1, \vec{x}_r^T)^T$ which serves as a basic vector for the one-dimensional solution space.

2.4. Observability

There exist restrictions on the observability of the quantities to be estimated.

If the spacecraft rotates around one of its principal axes, the resulting angular momentum vector is parallel to the angular velocity vector, cf. [23]. As an example, consider a cylindrical body which

rotates around its symmetry axis. Without loss of generality, we assume the axis to be the x-axis of the body system. In this case, the angular velocity $\vec{\omega}^{BF} = (\omega_1^{BF}, 0, 0)^T \in \mathbb{R}^3$ is an eigenvector of the inertia matrix I and only one parameter can be observed from that motion.

Considering the estimation of the center of mass position, the matrices defined in Eq. 8 do not have full rank if the body rotates for example around its x-body-axis. In this case, the linear system Eq. 6 does not have a unique solution. Measuring N angular velocities, the dimension of the space spanned by the angular velocity vectors must be equal to 3 such that the system is uniquely solvable.

This is why the full inertia properties and the center of mass can be determined only in the *nutation* case, i.e. if the nutation angle, defined as the angle between $\vec{h}$ and $\vec{\omega}$ [23], is bigger than zero. If the body rotates around one of its principal axis (*pure rotation* [23]), some of the inertia parameters are not observable.

An important fact is that the absolute value of the moment of inertia I cannot be estimated from torque-free motions. Let $\vec{h}^{IRF}$ denote as above the angular momentum vector in the inertial reference system. Only the vector

$$\left(\frac{I_{12}}{I_{11}}, \frac{I_{13}}{I_{11}}, \frac{I_{22}}{I_{11}}, \frac{I_{23}}{I_{11}}, \frac{I_{33}}{I_{11}}, \frac{h_1^{IRF}}{I_{11}}, \frac{h_2^{IRF}}{I_{11}}, \frac{h_3^{IRF}}{I_{11}}\right) \in \mathbb{R}^8 \tag{22}$$

can be observed. Thus, observing an unknown target which is freely tumbling in space, only the relationship between the principal moments of inertia can be determined, not their absolute values. This is in agreement with [24], where the authors also consider inertia ratios. Also in [15], only the ratios of the moments of inertia could be determined. The scale factor (recall definition of the solution space Eq. 20) can be found only when applying known forces and torques to the satellite and observing its resulting motion [15]. This is not possible when observing a passive target satellite from a safe distance which is freely tumbling without any external forces and torques acting on it.

3. Results

3.1. Generation of Test Data

The motion is generated by solving the quaternion differential equation and Euler equation for a given orientation and angular velocity at time $t = 0$, cf. [23]. The quaternion differential equation is

$$\frac{\mathrm{d}}{\mathrm{d}t}\vec{q}^{IRF} = \frac{1}{2}\Omega(\vec{\omega}^{IRF})\vec{q}^{IRF}, \tag{23}$$

where $\Omega(\vec{\omega}^{IRF}) \in \mathbb{R}^{4\times 4}$ is defined as

$$\Omega(\vec{\omega}^{IRF}) = \begin{pmatrix} 0 & \omega_3^{IRF} & -\omega_2^{IRF} & \omega_1^{IRF} \\ -\omega_3^{IRF} & 0 & \omega_1^{IRF} & \omega_2^{IRF} \\ \omega_2^{IRF} & -\omega_1^{IRF} & 0 & \omega_3^{IRF} \\ -\omega_1^{IRF} & -\omega_2^{IRF} & -\omega_3^{IRF} & 0 \end{pmatrix}. \tag{24}$$

In the absence of external torques, the Euler equation is given by

$$I\frac{\mathrm{d}}{\mathrm{d}t}\vec{\omega}^{IRF} = -\vec{\omega}^{IRF} \times (I\vec{\omega}^{IRF}). \tag{25}$$

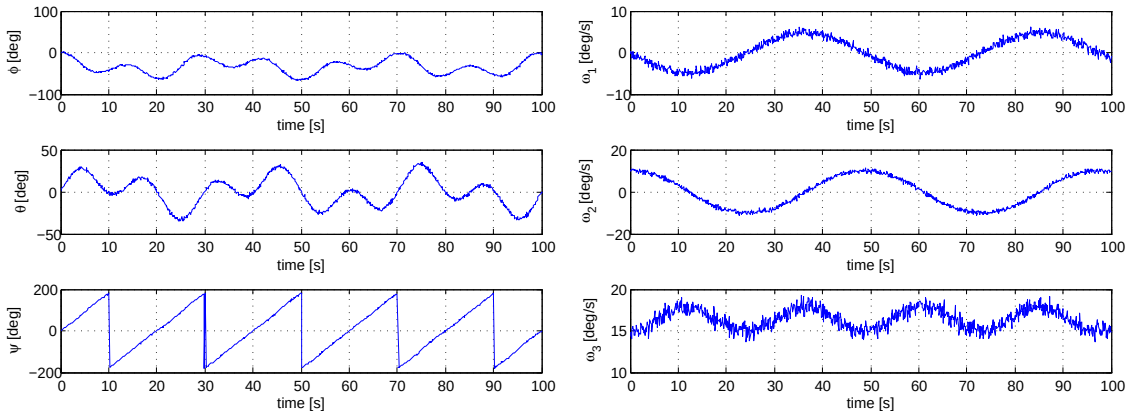

Figure 3. Measurements of Euler Angles [deg] (left) and Angular Velocity [deg/s] (right) for Test 1

Again, considering the Euler equation, any multiply of an inertia matrix I solves the equation with the same angular velocity $\vec{\omega}^{IRF}$. Observing torque-free motions, the moments of inertia can be determined only up to a multiplicative factor.

The ordinary differential equations are solved applying the explicit Euler scheme with a time step size of 0.004s. Measurements are simulated and taken every 0.1s by adding Gaussian noise to the real values.

The velocity of the geometrical center in the inertial frame is computed using the kinematic equation

$$\vec{v}^{IRF} = \vec{v}^{IRF}_{CoM} - \vec{\omega}^{IRF} \times \left((R^{BF}_{IRF})^T \vec{p}^{BF}_{CoM} \right), \tag{26}$$

where R^{BF}_{IRF} is the rotational matrix corresponding to the quaternion $\vec{q}^{IRF}$ and $\vec{v}^{IRF}_{CoM}$ is the velocity of the center of mass in the inertial reference frame. The position of the geometrical center in the inertial frame is obtained by numerical integration. The measurements are computed by adding again Gaussian noise.

Test values for the inertia tensor I and the position of the center of mass in the body system $\vec{p}^{BF}_{CoM}$ are chosen for different experiments and compared with the estimated values.

3.2. Experiments

3.2.1. Test 1 - First demonstration

For a first test, a rotation (cp. Fig. 3) is generated as described in Section 3.1. The figure presents measurements of the Euler angles of the rotation (convention 123) and measurements of the angular velocity $\vec{\omega}^{IRF}(t)$, $t \in [0,T]$ with $T = 100$s. The initial angular velocity is set to $\vec{\omega}^{IRF}(0) = (0,10,15)^T$ degrees per second. Since the observation time is $100s$ this results in $3-4$ full rotations. The position of the center of mass in the inertial reference frame are set to a constant value and its velocity to zero.

For this experiment, the center of mass is the geometrical center of the body, i.e. its position in the

body system is $\vec{p}_{CoM} = (0,0,0)^T$. The true inertia matrix for this test is set to

$$I = \begin{pmatrix} 34.1667 & 0 & 0 \\ 0 & 346.6667 & 0 \\ 0 & 0 & 354.1667 \end{pmatrix}. \tag{27}$$

As we can determine the moments of inertia only up to a multiplicative factor, we project the vector $\vec{I} := (I_{11}, I_{12}, I_{13}, I_{22}, I_{23}, I_{33}) \in \mathbb{R}^6$ to the sphere $\mathscr{S} = \left\{\vec{x} \in \mathbb{R}^6 : \|\vec{x}\| = 1\right\}$. The resulting vector is

$$\vec{I}_{\text{norm}} = (0.0688, 0, 0, 0.6978, 0, 0.7129)^T. \tag{28}$$

For simulating measurements, noise is added to the real data. For this test we use as standard derivative of the noise 1e$-$2 rad/s for the angular velocity and 1e$-$2 for the quaternion noise, and 1e$-$2 m/s for the velocity measurement of the translational motion of the geometrical center. The noise values correspond to experience with real measurement noise using rendezvous sensors like cameras [21].

The center of mass is estimated as described in Section 2.2. For this, $N = 1000$ measurements taken every 0.1s are considered. The resulting estimation of the position of the center of mass in the body frame is

$$\vec{p}^{BF}_{CoM} = (-0.00311, 0.00020, -0.00033)^T. \tag{29}$$

Therefore, the position of the center of mass has been estimated up to approximately 3 mm accuracy.

The moments of inertia are estimated as described in Section 2.3. The singular values of the matrix B are determined as

$$\Sigma = \{358.4657, 334.6122, 333.7640, 31.3929, 28.0363, 8.9168, 5.7866, 0.6387, 0.0427\}. \tag{30}$$

The smallest singular value 0.0427 is reset to 0, such that the modified matrix $\tilde{B}$ has rank 8. To find a basis vector of the solution space of $\tilde{B}\vec{x} = 0$, we set as described above $\vec{x}_1 = 1$ and compute the reduced vector $\vec{x}_r \in \mathbb{R}^8$. The solution of Eq. 21 is

$$\vec{x}_r = (-0.0149, -0.0110, 10.6631, 0.0063, 10.9355, -0.0047, 1.8568, 2.8642)^T. \tag{31}$$

Recall that the first six elements of $\vec{x} = (1, \vec{x}_r^T)^T \in \mathbb{R}^9$ are the moments of inertia; the last three elements are the components of the angular momentum. The resulting inertia written as 6D vector is thus

$$\vec{I}^{\text{est}} = (1, -0.0149, -0.0110, 10.6631, 0.0063, 10.9355)^T. \tag{32}$$

In order to compare the result with $\vec{I}_{\text{norm}}$, we normalize it

$$\vec{I}^{\text{est}}_{\text{norm}} := \vec{I}^{\text{est}} / \|\vec{I}^{\text{est}}\| = (0.0653, -0.0010, -0.0007, 0.6966, 0.0004, 0.7144)^T. \tag{33}$$

The estimation error is

$$\vec{I}^{\text{est}}_{\text{norm}} - \vec{I}_{\text{norm}} = (-0.0035, -0.0010, -0.0007, -0.0012, 0.0004, 0.0015)^T. \tag{34}$$

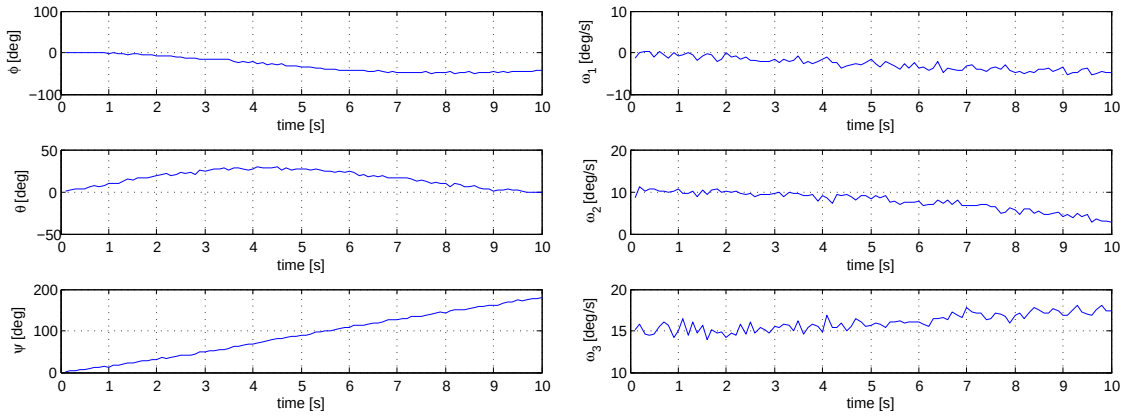

Figure 4. Measurements of Euler Angles [deg] (left) and Angular Velocity [deg/s] (right) for Test 2

3.2.2. Test 2 - Influence of the observation time

We used the same test data as in Test 1, but use only the first $N = 100$ measurements, which correspond to $T = 10$ seconds observation time. This results in less than a half rotation. Fig. 4 shows the measured orientation and angular velocity.

The center of mass is estimated as

$$\vec{p}_{CoM}^{BF} = (-0.0021, 0.1257, 0.1688)^T. \tag{35}$$

Concerning the position of the center of mass there is a high estimation error of 12.6 cm and 16.9 cm in the y- and z-component. Considering the data plotted in Fig. 4, the angular velocity changes only slightly in the 10 seconds of observation. Considering the data of the first test (see Fig. 3), the angular velocity is oscillating. After 50 seconds the angular velocity is approximately equal to the initial value of $\vec{\omega}^{IRF}(0) = (0, 10, 15)^T$ deg/s. Thus, the observation time has to be sufficiently long such that the estimation errors are in an acceptable range (e.g. mm range). This also matches with theoretical considerations: The nutation frequency [23] in rad/s is

$$W_n = \sqrt{\frac{(I_{11} - I_{33})(I_{22} - I_{33})}{I_{11} I_{22}}}\, \vec{\omega}^{IRF}(0)_3 = 0.1178. \tag{36}$$

The corresponding time is

$$T_n = \frac{2\pi}{W_n} = 53.3167. \tag{37}$$

The observation time should be once or twice the time interval of one full nutation T_n such that all parameters can be observed.

Considering the computed singular values of B for $N = 100$, it can be seen that the matrix is close to a matrix of rank 5 as there are 4 singular values close to zero.

$$\Sigma = \{37.7896, 36.9529, 34.7566, 0.2883, 0.1841, 0.0071, 0.0066, 0.0030, 0.0026\}. \tag{38}$$

Adapting only the smallest eigenvalue to enforce rank 8 leads to the following estimation of the normalized inertia:

$$\vec{I}_{\text{norm}}^{\text{est}} = (0.9731, 0.0010, 0.0619, 0.0201, -0.0007, 0.2211)^T . \tag{39}$$

This results in a high estimation error of

$$\vec{I}_{\text{norm}}^{\text{est}} - \vec{I}_{\text{norm}} = (0.9043, 0.0010, 0.0619, -0.6777, -0.0007, -0.4918)^T . \tag{40}$$

Another experiment using the same test data with $T = 300$, i.e. with $N = 3000$ measurements, is performed. The center of mass is estimated as

$$\vec{p}_{CoM}^{BF} = (-0.00043, 0.00111, 0.00029)^T . \tag{41}$$

The estimated, normalized inertia is

$$\vec{I}_{\text{norm}}^{\text{est}} = (0.0727, 0.0005, 0.0004, 0.6988, -0.0006, 0.7116)^T . \tag{42}$$

This results in an estimation error of

$$\vec{I}_{\text{norm}}^{\text{est}} - \vec{I}_{\text{norm}} = (0.0039, 0.0005, 0.0004, 0.0010, -0.0006, -0.0013)^T . \tag{43}$$

Comparing these results with those of $N = 1000$, the accuracy could not be significantly improved. Therefore, a longer observation is not necessary. It may be advantageous only if the measurement noise is higher. In this case, collecting more data could improve the estimation result.

To investigate this, we use again the same test data as in Test 1 but increase the measurement noise by a factor of 5. We compare the results gained for $N = 1000, 5000$ and 10000 measurements. Table 1 shows a comparison of the absolute error of the center of mass position estimation and the inertia estimation. This demonstration shows that by adding more measurements the accuracy can be increased. However the bigger the noise, the more measurements need to be taken in account and the computational effort increases.

Table 1. Comparison of the performance dependent on the number of measurements

Number of Meas.	1000	5000	10000
Error $\vec{p}_{CoM}^{BF}$	0.0018	0.0003	0.0002
	0.0238	0.0075	0.0050
	0.0115	0.0093	0.0013
Error $\vec{I}_{\text{norm}}$	0.0617	0.0507	0.0276
	0.0321	0.0044	0.0000
	0.0123	0.0009	0.0000
	0.0282	0.0127	0.0110
	0.0090	0.0078	0.0001
	0.0387	0.0196	0.0142

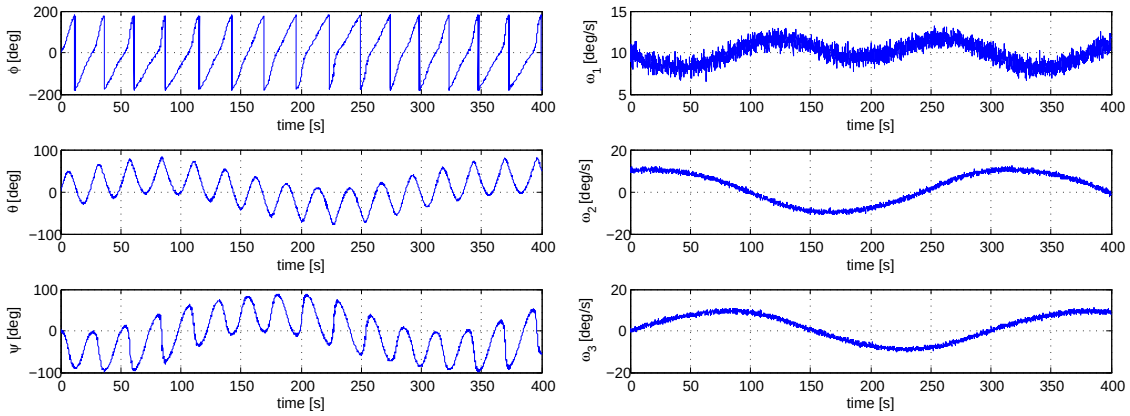

Figure 5. Measurements of Euler Angles [deg] (left) and Angular Velocity [deg/s] (right) for Test 3

3.2.3. Test 3 - Non-diagonal inertia matrix and center of mass deviation

In another experiment we consider an inertia matrix of the form

$$I = \begin{pmatrix} 121 & 0.4 & 0.3 \\ 0.4 & 109 & 4.5 \\ 0.3 & 4.5 & 106 \end{pmatrix}. \tag{44}$$

The non-diagonal entries are now non-zero. Rewritten as a 6D vector and projected to the sphere $\mathscr{S}$, we obtain

$$\vec{I}_{\text{norm}} = (0.6225, 0.0021, 0.0015, 0.5608, 0.0232, 0.5454)^T. \tag{45}$$

Further, we consider a center of mass which is not the geometrical center of the body. Its position with respect to the body frame is

$$\vec{p}_{CoM}^{\,BF} = (0.8, 0.3, 0.05)^T. \tag{46}$$

For simulating measurements, noise as in Test 1 is added to the real data; the measurements are shown in Fig. 5. As the period is longer for this experiment, we observed the motion for 400 seconds. The center of mass position is estimated as

$$\vec{p}_{CoM}^{\,BF} = (0.79544, 0.29843, 0.04971)^T \tag{47}$$

which is again accurate up to an error of about 5 mm. The estimated moments of inertia normalized to 1 are

$$\vec{I}_{\text{norm}}^{\text{est}} = (0.6218, 0.0027, 0.0008, 0.5599, 0.0220, 0.5472)^T. \tag{48}$$

This results in an estimation error of

$$\vec{I}_{\text{norm}}^{\text{est}} - \vec{I}_{\text{norm}} = (-0.0007, 0.0006, -0.0007, -0.0009, -0.0012, 0.0018)^T. \tag{49}$$

4. Discussion

The center of mass can be estimated with an accuracy of a few millimeter. The error of the normalized moments of inertia is of magnitude $1e-3$.

The observation time plays a critical role. If the overall time frame is too short, the resulting equations cannot be solved as there are not enough linear independent measurements. Concerning the center of mass computation for instance, the term $W_i^{IRF}\,(R_{i,IRF}^{BF})^T$ will change only little and the involved matrix A in Eq. 7 will be close to a singular matrix.

The full set of parameters can only be observed in the nutation case, not from pure rotation, cf. Section 2.4.. One or two complete periods of rotation and of the resulting nutation of the target have to be observed, cf. Section 3.2.

Beyond that, the number of measurements influence the accuracy especially if the measurement noise is high. In this case, additional measurements are necessary to improve the estimation based on a least squares optimization.

We therefore recommend to include an inspection phase in an on-orbit servicing mission which takes sufficiently long dependent on the period of the angular velocity and dependent on the magnitude of the measurement noise.

No significant correlation can be noted concerning the performance of this method and the position of the center of mass or the symmetry of the body. Test 3 showed that also non-diagonal, more complex inertia tensors can be estimated with the same performance as in Test 1 where the inertia matrix was diagonal. Also no influence of the distance of the mass center from the geometrical center has been noticed.

5. Conclusion

We presented a method for estimating the center of mass position and the moments of inertia of a freely tumbling, passive satellite. The method uses processed data from optical sensors like cameras or LIDARs. The estimation is based on kinematic equations and the conservation of the angular momentum and leads to least squares problems. Concerning the estimation of the inertia tensor, we solve a constrained least squares problem to ensure positive diagonal values of the inertia matrix. Additionally, we proposed to analyze the singular values of the involved matrices to avoid numerical problems concerning the rank of matrices caused by measurement noise and numerical rounding errors.

Further, we analyzed the accuracy of the estimations. Besides noise, the accuracy is mainly dependent on the duration of the observation compared to the period of the rotation and nutation of the observed body.

An important application of the methods presented in this paper are on-orbit servicing missions where a service satellite approaches a non-cooperative target satellite whose center of mass and

inertia parameters are unknown. For a safe approach and docking to the target, we recommend to include an inspection phase where the satellite is observed from a safe distance and the unknown inertia parameters are estimated as described in this work.

A next step in this research is the use of real sensor data from cameras or LIDARs in a hardware-in-the-loop framework. This will result in a more realistic scenario with non-artificial measurement noise.

6. References

[1] Kaiser, C., Sjberg, F., Delcura, J. M., and Eilertsen, B. "SMART-OLEV - An Orbital Life Extension Vehicle For Servicing Commercial Spacecrafts in GEO." Acta Astronaut., Vol. 63, No. 1-4, 2008.

[2] Ellery, A., Kreisel, J., and Sommer, B. "The Case for Robotic On-Orbit Servicing of Spacecraft: Spacecraft Reliability is a Myth." Acta Astronaut., Vol. 63, No. 5-6, 2008.

[3] Stoll, E., Letschnik, J., Walter, U., Artigas, J., Kremer, P., Preusche, C., and Hirzinger, G. "On-Orbit Servicing." IEEE Robot. Autom. Mag., Vol. 16, No. 4, 2009.

[4] Nishida, S.-I., Kawamoto, S., Okawa, Y., Terui, F., and Kitamura, S. "Space Debris Removal System Using a Small Satellite." Acta Astronaut., Vol. 65, No. 1-2, 2009.

[5] Xu, W., Liang, B., Li, C., and Xu, Y. "Autonomous Rendezvous and Robotic Capturing of Non-Cooperative Target in Space." Robotica, Vol. 28, No. 5, 2010.

[6] Du, X., Liang, B., Xu, W., and Qiu, Y. "Pose Measurement of Large Non-cooperative Satellite Based on Collaborative Cameras." Acta Astronaut., Vol. 68, p. 20472065, 2011.

[7] Ma, O., Flores-Abad, A., and Boge, T. "Use of industrial robots for hardware-in-the-loop simulation." Acta Astronaut., Vol. 81, No. 1, 2012.

[8] Qiao, B., Tang, S., Ma, K., and Liu, Z. "Relative pose and attitude estimation of spacecrafts based on dual quaternion for rendezvous and docking." Acta Astronaut., Vol. 91, 2013.

[9] Feldman, A. and Lee, A. Y. "In-Flight Estimations of Cassini Spacecraft Inertia Tensor and Thruster Magnitude." "Proceedings of the 16th AAS/AIAA Space Flight Mechanics Conference," Tampa, Florida, 2006.

[10] Keim, J. A., Acikmese, B. A., and Shields, J. F. "Spacecraft Inertia Estimation via Constrained Least Squares." "Proceedings of the IEEE Aerospace Conference," Big Sky, Montana, 2006.

[11] Ma, O., Dang, H., and Pham, K. "On-Orbit Identification of Inertia Properties of Spacecraft Using a Robotic Arm." J. Guid. Control Dynam., Vol. 31, No. 6, 2008.

[12] Kim, D. H., Choi, D.-G., and Oh, H.-S. "Inertia Estimation of Spacecraft Based on Modified Law of Conservation of Angular Momentum." Astrophys. Space Sci., Vol. 27, No. 4, 2010.

[13] Benninghoff, H., Boge, T., and Tzschichholz, T. "Hardware-in-the-Loop Rendezvous Simulation Involving an Autonomous Guidance, Navigation and Control System." Adv. Astronaut. Sci., Vol. 145, 2012.

[14] Benninghoff, H., Boge, T., and Rems, F. "Autonomous Navigation for On-Orbit Servicing." KI - Künstliche Intelligenz, Vol. 28, No. 2, pp. 77–83, 2014.

[15] Sheinfeld, D. and Rock, S. M. "Rigid Body Inertia Estimation with Applications to the Capture of a Tumbling Satellite." Proceedings of the 19th AAS/AIAA Spaceflight Mechanics Meeting. Savannah, Georgia, 2009.

[16] Nocedal, W. and Wright, S. J. Numerical Optimization. Springer Series in Operations Research. Springer, New York, 1999.

[17] Jasiobedzki, P., Greenspan, M., and G., R. "Pose Determination and Tracking for Autonomous Satellite Capture." Proceedings of the 6th International Symposium on Artificial Intelligence and Robotics & Automation in Space (i-SAIRAS). St-Hubert, Quebec, Canada, 2001.

[18] Jasiobedzki, P., Se, S., Pan, T., Umasuthan, M., and Greenspan, M. "Autonomous Satellite Rendezvous and Docking Using LIDAR and Model Based Vision." Vol. 54 of *SPIE 5798, Spaceborne Sensors II*. 2005.

[19] Shahid, K. and Okouneva, G. "Intelligent LIDAR scanning region selection for satellite pose estimation." Comput. Vis. Image Underst., Vol. 107, No. 3, 2007.

[20] Mark, L., Okouneva, G., Saint-Cyr, P., Ignakov, D., and English, C. "Near-Optimal Selection of Views and Surface Regions for ICP Pose Estimation." "Advances in Visual Computing," Vol. 6454 of *Lecture Notes in Computer Science*. Springer Berlin Heidelberg, 2010.

[21] Boge, T., Benninghoff, H., and Tzschichholz, T. "Visual Navigation for On-Orbit Servicing Missions." Proceedings of the 5th Int. Conference on Spacecraft Formation Flying Missions and Technologies. Munich, Germany, 2013.

[22] Rems, F., González, J. A. M., Boge, T., Tuttas, S., and Stilla, U. "Fast Initial Pose Estimation of Spacecraft from LiDAR Point Cloud Data." Proceedings of the 13th Symposium on Advanced Space Technologies in Robotics and Automation. Noordwijk, The Netherlands, 2015.

[23] Wertz, J. R. Attitude Determination and Control. Kluwer Academic Publisher, Dordrecht, Boston, London, 2002.

[24] Aghili, F. and Parsa, K. "Motion and Parameter Estimation of Space Objects Using Laser-Vision Data." J. Guid. Control Dynam., Vol. 32, No. 2, 2007.